Arch. Mech., **53**, 4-5, pp. 487–499, Warszawa 2001

Material modeling of concrete subjected to multiaxial loading: application to pull-out analyses

P. PIVONKA, R. LACKNER, and H. A. MANG

Institute for Strength of Materials
Vienna University of Technology, Vienna, Austria

THIS PAPER DEALS with the application of 3D-constitutive models for concrete to simulations of pull-out experiments [1]. Two different models are considered:

- The first material model is formulated within the framework of multi-surface plasticity. It consists of three Rankine yield surfaces for the simulation of cracking and a Drucker-Prager yield surface for the description of compressive failure of concrete. The Drucker-Prager surface is reformulated in order to account for the influence of confinement on the compressive strength and the ductility of concrete.
- The formulation of the second model, the Extended Leon Model (ELM) [4], is based on one yield function for description of compressive and tensile failure of concrete. It accounts for the influence of the Lode angle on the material strength. The simulation of ductile behavior of concrete is controlled by means of a pressure-dependent ductility function.

The predictive capability of the models is demonstrated by means of a finite element (FE) analysis of a pull-out test [1]. The influence of confinement on the peak load and the failure mode is investigated.

Key words: concrete, triaxial loading, pull-out analyses, multi-surface plasticity, Drucker-Prager, Rankine, Extended Leon Model, confinement

1. Introduction

THE USE OF NUMERICAL tools such as the FEM allows simulation of real-life structures characterized by complex geometric properties and loading conditions. As regards the simulation of concrete structures, sophisticated material models are required in order to provide an appropriate description of the mechanical behavior of concrete. Such material models should account for crack opening in the case of tensile loading, crushing in the case of compressive loading, and compaction of concrete when subjected to hydrostatic pressure.

In the context of plasticity theory, failure may be described either by one failure criterion (single-surface plasticity) or by a combination of several failure criteria (multi-surface plasticity). As regards single-surface models, the ELM [4] was developed in order to give realistic results for tensile, compressive, and confined compressive states of loading. It is characterized by relating the main parameters of the model such as, e.g., ductility and fracture energy to the confinement of the material. The hydrostatic pressure is used as the measure for confinement.

In multi-surface plasticity, each failure criterion is used to describe a certain mode of material failure. For the simulation of cracking, the Rankine criterion gives the best results. In the compressive loading regime, the Drucker-Prager surface is commonly employed (see, e.g., [5][10]). The compaction of concrete may be considered by means of an additional cap (see, e.g., [7]).

In this paper, two material models developed for the simulation of the mechanical behavior of concrete, the Extended Leon Model [2] and a multi-surface plasticity model consisting of the Drucker-Prager criterion and the Rankine criterion, are considered. As regards the Drucker-Prager criterion, a reformulation is proposed in order to extend its range of applicability. The influence of this reformulation on the numerical results is demonstrated by means of a finite element analysis of a pull-out test.

In the following section, both material models are briefly presented and the proposed modification of the Drucker-Prager criterion is described. However, the main part of the paper is devoted to the numerical analysis of a pull-out test. The respective results are contained in Sec. 3.

2. 3D plasticity models for plain concrete

Concrete is a composite material, made of cement, aggregates, and water. In continuum mechanics, however, concrete is treated as homogeneous material. The respective scale of observation is referred to as macro-level. Stress-strain relations formulated at the macro-level relate macro-stresses to macro-strains. However, the mechanical behavior observed at the macro-level is associated with phenomena occurring at the micro-level of the material. E.g., inelastic macro-strains arise from micro-cracking of hydrates. For the description of phenomena at the micro-level, so-called internal variables $\boldsymbol{\alpha}$ are introduced in the material model. They are used to describe the microstructural change of the material. The energetically conjugated thermodynamic quantities are the hardening/softening forces $\mathbf{q}$. They are related to the internal variables via the state equation $\mathbf{q}=\mathbf{q}(\boldsymbol{\alpha})$. The hardening forces represent the actual strength of the material, defining the space of admissible stress states, $\mathbf{C}_E$

$$\boldsymbol{\sigma} \in \mathbf{C}_E \;\Leftrightarrow\; f_k = f_k(\boldsymbol{\sigma},\mathbf{q}(\boldsymbol{\alpha})) \leq 0 \quad \forall \quad k \in [1,2,\ldots,N], \tag{2.1}$$

where f_k denotes the k-th yield function. In definition (2.1), the general case of multi-surface plasticity is considered. N denotes the number of employed yield functions.

The internal variables and the respective deformations related to plastic material response are obtained by means of evolution equations, reading

$$\dot{\boldsymbol{\alpha}} = \sum_{k \in J_{act}} \dot{\gamma}_k \frac{\partial H_k}{\partial \mathbf{q}}, \quad \dot{\boldsymbol{\varepsilon}}^p = \sum_{k \in J_{act}} \dot{\gamma}_k \frac{\partial Qk}{\partial \boldsymbol{\sigma}}, \tag{2.2}$$

where γ_k denotes the plastic multiplier of the k-th yield function. Q_k and H_k are potentials which, in general, depend on $\boldsymbol{\sigma}$ and $\mathbf{q}$.

The first material model considered in this paper is formulated within the framework of multi-surface plasticity theory. It consists of four yield surfaces (N=4): a Drucker-Prager (DP) yield surface for the description of concrete when subjected to compressive loading and three Rankine (RK) surfaces for the description of tensile failure. In the principal stress space, the failure criteria read

$$f_{DP}(\boldsymbol{\sigma}, q_{DP}) = \sqrt{J_2} - \kappa_{DP} I_1 - \frac{\bar{q}_{DP}}{\beta_{DP}} \quad \text{with} \quad \bar{q}_{DP} = f_{cy} - q_{DP}, \tag{2.3}$$

and

$$f_{RK,A}(\sigma_A, q_{RK}) = \sigma_A - \bar{q}_{RK}, \quad \text{with} \quad \bar{q}_{RK} = f_{tu} - q_{RK}, \tag{2.4}$$

where the subscript "A"(A=1,2,3) refers to one of the three principal axes. f_{tu} is the tensile strength and f_{cy} represents the elastic limit of concrete under uniaxial compressive loading. κ_{DP} and β_{DP} are constant material parameters.

For the description of microstructural changes of concrete, two internal variables are employed: α_{RK} and α_{DP}. They are computed according to associated hardening/softening laws, i.e., $H_{RK,A}$=$f_{RK,A}$ and H_{DP}=f_{DP}, reading

$$\dot{\alpha}_{RK} = \sum_{A=1}^{3} \dot{\gamma}_{RK,A} \frac{\partial f_{RK,A}}{\partial q_{RK}}, \quad \dot{\alpha}_{DP} = \dot{\gamma}_{DP} \frac{\partial f_{DP}}{\partial q_{DP}}. \tag{2.5}$$

Cracking of concrete is characterized by a continuous decrease of the tensile strength, $\bar{q}_{RK}$. Accordingly, an exponential softening law is chosen, reading

$$\bar{q}_{RK} = f_{tu} \exp[-\alpha_{RK}/\alpha_{RK,u}], \tag{2.6}$$

where $\alpha_{RK,u}$ is a calibration parameter. Under compressive loading, however, the behavior of concrete is characterized by hardening as well as softening behavior. The chosen hardening/softening curve for the compressive strength, $\bar{q}_{DP}$, is depicted in Fig. 1a. Commonly, the Drucker-Prager criterion is calibrated by

means of uniaxial and biaxial compression tests, giving β_{DP} and κ_{DP} (see, e.g., [11]). For the application of the Drucker-Prager criterion experiencing mainly biaxial stress states, this mode of calibration is appropriate. For confined stress states, however, large deviations between the experimental data and the numerical results were reported in [13]. Experimental data indicate an influence of confinement on both the compressive strength, described by the ultimate and the residual strengths, $\bar{q}_{DP,p}$ and $\bar{q}_{DP,r}$, and the ductility [14]. The proposed modification of the Drucker-Prager criterion accounts for this influence by relating $\bar{q}_{DP,p}$, $\bar{q}_{DP,r}$, and $\alpha_{DP,m}$ to the actual level of confinement. Confinement is represented by the major principal stress σ_1, with $\sigma_1 \geq \sigma_2 \geq \sigma_3$, yielding $\bar{q}_{DP,p} = \bar{q}_{DP,p}(\sigma_1)$, $\bar{q}_{DP,r} = \bar{q}_{DP,r}(\sigma_1)$, and $\alpha_{DP,m} = \alpha_{DP,m}(\sigma_1)$ (see Fig. 1b and 1c). $\bar{q}_{DP,p}$ and $\bar{q}_{DP,r}$ are computed by means of the Drucker-Prager criterion, $f_{DP} = 0$, using the stress state $\boldsymbol{\sigma}^T = [\sigma_1, \sigma_1, \sigma_3(\sigma_1)]$ (for details, see [13]).

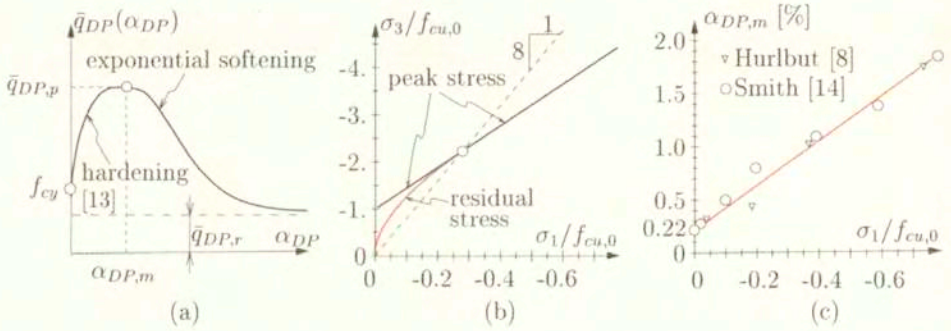

FIG. 1. Multi-surface model: (a) employed hardening/softening curve for the Drucker-Prager criterion; influence of confinement on (b) the peak and residual stress (related to $\bar{q}_{DP,p}$ and $\bar{q}_{DP,r}$) and (c) the ductility $\alpha_{DP,m}$. The level of confinement is represented by the maximum principal stress σ_1 (f_{cy}: elastic limit under uniaxial compressive loading, f_{cu}: uniaxial compressive strength of concrete)

The second material model considered in this paper is the Extended Leon Model (ELM) [2]. It belongs to the class of single-surface models, i.e., $N=1$. The yield function is given by

$$f_{ELM}(p,r,\theta;q_h,q_s) = \left\{\left(1-\frac{\bar{q}_h}{f_{cu}}\right)\left[\frac{p}{f_{cu}}+\frac{rg(\theta,e)}{\sqrt{6}f_{cu}}\right]^2+\sqrt{\frac{3}{2}}\frac{rg(\theta,e)}{f_{cu}}\right\}^2 + \left(\frac{\bar{q}_h}{f_{cu}}\right)^2 m(q_s)\left[\frac{p}{f_{cu}}+\frac{rg(\theta,e)}{\sqrt{6}f_{cu}}\right]-\left(\frac{\bar{q}_h}{f_{cu}}\right)^2\frac{\bar{q}_s}{f_{tu}}=0, \tag{2.7}$$

with

$$\bar{q}_h = f_{cy} - q_h \quad \text{and} \quad \bar{q}_s = f_{tu} - q_s. \tag{2.8}$$

In Eq. (2.7), p is the hydrostatic pressure, r is the deviatoric radius, and θ denotes the Lode angle. f_{cu} and f_{tu} denote the uniaxial compressive and tensile strength, respectively. The deviatoric shape of the loading surface is described by the elliptic function $g(\theta, e)$ (see [15]), where the parameter e is referred to as eccentricity, describing the out-off roundness of the deviatoric meridian. $m(q_s)$ is a frictional parameter. The ELM is used for the simulation of hardening as well as softening material response. Hence, two hardening/softening forces, q_h and q_s, are contained in the yield function (2.7). The internal variables, α_h and α_s, are employed to monitor the respective changes of the material at the micro-level. The evolution equations for α_h and α_s are given as [13]

$$\dot{\alpha}_h = \dot{\gamma} \frac{\partial H_{ELM,h}}{\partial q_h} = \frac{1}{x_h(p)} \dot{\epsilon}_h^p \quad \text{with} \quad \dot{\epsilon}_h^p = \dot{\gamma} \, \| \frac{\partial Q_{ELM}}{\partial \sigma} \|, \tag{2.9}$$

$$\dot{\alpha}_s = \dot{\gamma} \frac{\partial H_{ELM,s}}{\partial q_s} = \frac{1}{x_s(p)} \dot{\epsilon}_s^p \quad \text{with} \quad \dot{\epsilon}_s^p = \dot{\gamma} \, \| \langle \frac{\partial Q_{ELM}}{\sigma} \rangle \|. \tag{2.10}$$

In Eq. (2.10), the McAuley operator $\langle \bullet \rangle = (\bullet + |\bullet|)/2$ extracts the positve eigenvalues of the principal components of $\partial Q_{ELM}/\partial \sigma$ [12]. x_h and x_s are pressure-dependent ductility functions in the hardening and the softening regime, respectively. The influence of the ductility function on the hardening and softening material behavior is illustrated in Fig. 2.

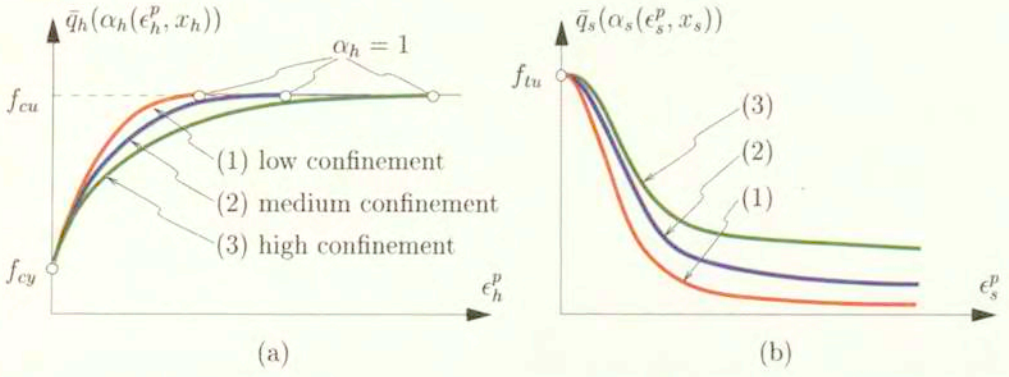

FIG. 2. Extended Leon Model: illustration of the influence of (a) the ductility function x_h on the increase of the compressive strength $\bar{q}_h$ and (b) the ductility function x_s on the decrease of the residual strenght $\bar{q}_s$ (f_{cy}: elastic limit under compresive loading, with $f_{cy} = 0.2 \, f_{cu}$)

3. Failure analysis of pull-out test

The focus of the present paper is on the influence of the underlying material model on the numerical results obtained from failure analyses of anchor bolts in concrete, referred to as the pull-out test. For this purpose, analyses on the basis of both material models described in Sec. 2 were performed. Moreover, the influence of confinement on the peak load and on the failure mode is investigated.

3.1. Geometric dimensions and material properties

Figure 3 contains the experimental setup of the considered pull-out test (Round-Robin test [1]). It shows the geometric dimensions as well as the support conditions of the specimen. Further, the material properties of concrete and steel are given.

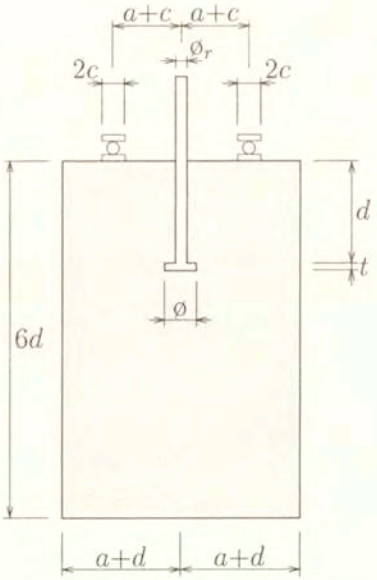

dimensions:
d=150 mm a=150 mm
t=15 mm c=22.5 mm
ø=45 mm $ø_r$=24 mm

concrete:
Young's modulus: E_c=30000 N/mm^2
Poisson's ratio: ν_c=0.2
uniaxial compressive strength: f_{cu}=40 N/mm^2
uniaxial tensile strength: f_{tu}=3 N/mm^2
fracture energy: G_f^I=0.1 Nmm/mm^2
fracture energy: G_f^{II}=50G_f^I

steel:
Young's modulus: E_s=210000 N/mm^2
Poisson's ratio: ν_s=0.3

FIG. 3. Pull-out analysis: geometric dimensions and material properties

3.2. Numerical analysis

In the numerical analysis, the material behavior of the steel bolt is assumed to be linear elastic. For the description of concrete, the two previously described material models are used.

Because of symmetry of the geometric dimensions and the loading conditions, the problem is solved by means of axisymmetric analyses. Fig. 4 shows

the employed FE mesh consisting of 677 four-node finite elements. As regards the mechanical model of the anchor bolt, only the anchor head is discretized. At the contact line between the anchor head and the concrete, no slip is considered. The analyses are performed displacement-driven. The displacement at the nodes of the anchor head located at the axis of symmetry is prescribed (see Fig. 4).

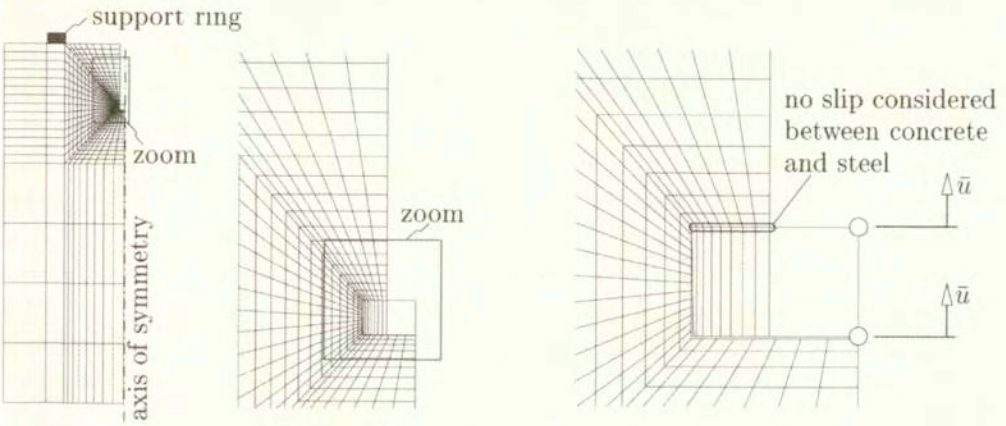

FIG. 4. Pull-out analysis: FE discretization

Softening functions appearing in the formulations of both models were calibrated according to the fictitious crack concept [6]. The application of the fictitious crack concept to the simulation of radial cracks in axisymmetric analyses requires the input of the expected number of radial cracks (for details, see [9]). In the present analyses, four radial cracks are assumed to develop.

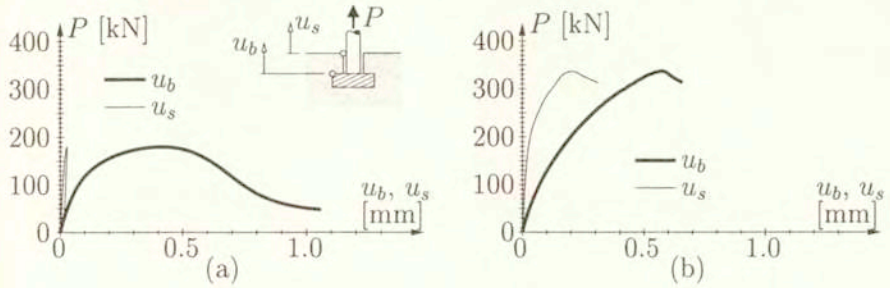

FIG. 5. Pull-out analysis: (a) load-displacement curves obtained from multi-surface model with (a) *original* and (b) *modified* Drucker-Pager criterion

Figure 5 contains the load-displacement curves obtained from the multi-surface model. The peak load obtained from the Drucker-Prager criterion characterized by consideration of confinement (*modified* model) was found to be 340 kN.

Neglection of the influence of confinement within the Drucker-Prager criterion (*original* model), i.e., setting $\bar{q}_{DP,p}$=const., $\bar{q}_{DP,r}$=const., and $\alpha_{DP,m}$=0.0022, led to a reduction of the peak load by 47% (see Fig. 5a). The difference between the displacement at the anchor head and the concrete surface, $u_b - u_s$, is an indicator for compressive failure of concrete over the anchor head. An almost constant evolution of $u_b - u_s$ indicates a rigid body motion in consequence of formation of a cone-like failure mode (see, e.g., Fig. 8a). Small values of u_s together with continuously increasing values of $u_b - u_s$ indicate local failure of concrete over the anchor head. This failure mode was obtained from the analysis based on the *original* multi-surface model (see Fig. 5a). The underestimation of compressive strength and ductility by neglecting the influence of confinement resulted in compressive failure of concrete over the anchor head. The respective $P - u_b$ curve shows similar characteristics as the underlying hardening/softening curve used for the Drucker-Prager criterion (see Fig. 1a). Moreover, failure of concrete over the anchor head resulted in an unloading of the remaining part of the structure. This is reflected by the decrease of u_s in the post-peak regime. Consideration of confinement by the *modified* multi-surface model led to an increase of the compressive strength over the anchor head. The almost constant evolution of $u_b - u_s$ in the post-peak regime indicates the development of a cone-like failure mode (see Fig. 8a).

The distribution of α_{DP} is given in Fig. 6 for both analyses at the respective peak loads. The compressive failure over the anchor head obtained from the *original* model is reflected by softening material behavior (see Fig. 6a).

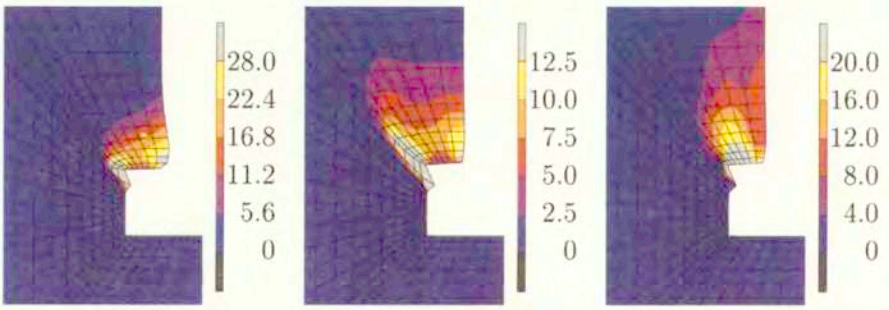

(a) $10^3 \cdot \alpha_{DP}$ (b) $10^3 \cdot \alpha_{DP}$ (c) $10^3 \cdot \alpha_{DP,m}$

FIG. 6. Pull-out analysis: distribution of the internal hardening/softening variable of the Drucker-Prager criterion, α_{DP}, at peak load obtained from (a) *original* and (b) *modified* multi-surface model; (c) distribution of $\alpha_{DP,m}$ at peak load obtained from *modified* multi-surface model (10-fold magnification of displacements)

Softening is characterized by $\alpha_{DP} > \alpha_{DP,m}$=0.0022. On the other hand, the confinement considered in the simulation based on the *modified* multi-surface

model resulted in an increase of $\alpha_{DP,m}$ over the anchor head (see Fig. 6c). The distribution of α_{DP} is shown in Fig. 6b. The values of α_{DP} are lower than the respective values of $\alpha_{DP,m}$ indicating that the compressive strength in this area has not reached the ultimate strength $\bar{q}_{DP,p}$ (hardening regime). The strong influence of confinement on the obtained numerical results is a consequence of large compressive stresses over the anchor head. For the multi-surface model, the major principal stress is used as a measure for confinement. If the major principal stress is positive, no confinement is considered. Fig. 7 shows the distribution of the two principal stresses in the axisymmetric plane, denoted as σ_{min} and σ_{max}, and the circumferential stress σ_{circ} at peak load obtained from the analysis based on the *modified* multi-surface model. Over the anchor head, negative stresses are observed for all three principal stresses. Hence, $\sigma_1 < 0$, resulting in an increase of the compressive strength and the ductility (see Fig. 1b and 1c).

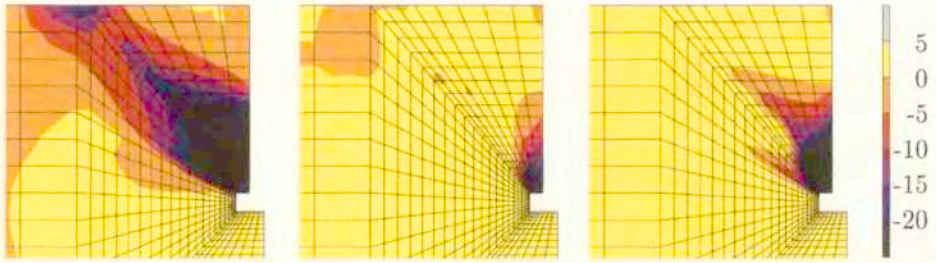

FIG. 7. Pull-out analysis: distribution of principal stresses in the axisymmetric plane, σ_{min} and σ_{max}, and the stress component in the circumferential direction, σ_{circ}, at peak load obtained from *modified* multi-surface model (in [N/mm^2])

The distribution of the minimum in-plane principal stress σ_{min} (see Fig. 7a) provides insights into the load-carrrying behavior of the concrete specimen. The applied load at the anchor head is transferred by a compressive strut from the confined area over the anchor head to the support ring (see [3] for similar results). The respective maximum principal stress in this strut resulted in the development of a circumferential crack. This crack started to open at the anchor head propagating towards the support ring, finally causing a cone-shaped failure of the specimen. The crack pattern obtained at peak load on the basis of the *modified* multi-surface model is shown in Fig. 8a by means of the distribution of the maximum plastic strain in the axisymmetric plane, ε^p_{max}. In addition to the circumferential crack, radial cracks developed, starting from the corner at the concrete surface and propagating into the interior of the concrete block. Recall, four radial cracks were assumed to open in the context of the fictitious crack

concept. In Fig. 8b, the location of these radial cracks is shown by means of the respective circumferential plastic strain, ε^p_{circ}.

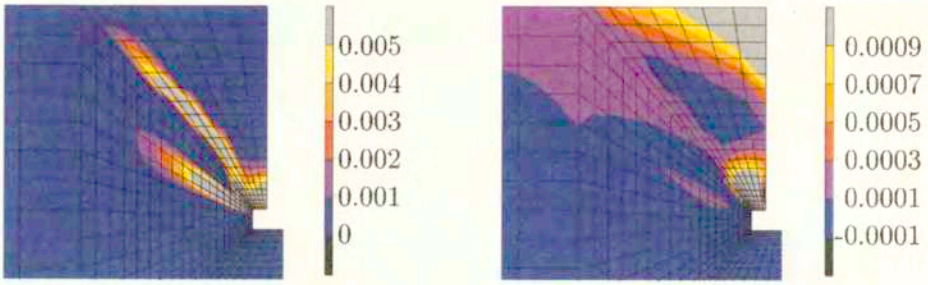

(a) ε^p_{max} (b) ε^p_{circ}

FIG. 8. Pull-out analysis: distribution of the maximum plastic strain in axisymmetric plane, ε^p_{max}, and of the circumferential plastic strain ε^p_{circ} at peak load obtained from *modified* multi-surface model

The load displacement curve obtained from the analysis based on the single-surface model is shown in Fig. 9. The peak load was computed as 312 kN. The continuously increasing value of $u_b - u_s$ in the pre-peak regime indicates plastic material response over the anchor head. However, the actual failure occurs in consequence of circumferential cracks resulting in a cone-like failure surface. Similar to the analysis based on the *modified* multi-surface model, an almost constant evolution of $u_b - u_s$ is observed in the post-peak regime indicating this mode of failure.

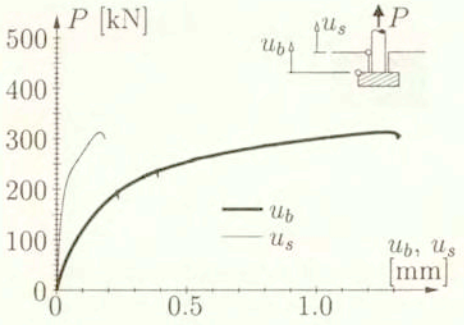

FIG. 9. Pull-out analysis: load displacement curve obtained from single-surface model

The distribution of α_h at peak load is shown in Fig. 10a. α_h describes the state of the yield surface in the hardening regime. $\alpha_h = 0$ refers to the initial yield surface defined by $\bar{q}_h = f_{cy}$ (see Fig. 2a.) If $\alpha_h = 1$, the failure surface is reached ($\bar{q}_h = f_{cu}$) and softening or ideally-plastic behavior is initiated. Whether or not

softening will take place depends on the level of confinement. For the single-surface model, confinement is represented by the hydrostatic pressure. For a hydrostatic pressure p, with $p = -(\sigma_1 + \sigma_2 + \sigma_3)/3$, lower than the hydrostatic pressure related to the so-called transition point TP, p_{TP}, softening occurs. For stress states characterized by $p > p_{TP}$, ideally-plastic material behavior is assumed. The transition point TP is equal to the stress point on the failure surface characterized by a confined stress state given as $\sigma_1 = \sigma_2$, $\sigma_3 = 8\sigma_1$ [14]. Based on the material parameters given in Fig. 3, the hydrostatic pressure at the TP is computed as p_{TP}=44.3 N/mm^2.

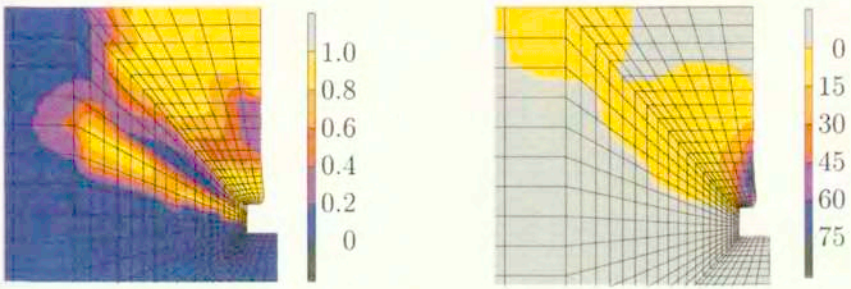

FIG. 10. Pull-out analysis: distribution of (a) the internal hardening variable α_h and (b) the hydrostatic pressure p, with $p = -(\sigma_1 + \sigma_2 + \sigma_3)/3$, (in [N/mm^2]) at peak load obtained from single-surface model (5-fold magnification of displacements)

The distribution of the hardening variable α_h at peak load shown in Fig. 10a is characterized by several zones with $\alpha_h = 1$. As regards the zone over the anchor head, the respective hydrostatic pressure is greater than the hydrostatic pressure at the transition point, i.e., $p > p_{TP}$. This resulted in ideally-plastic material response and, hence, in plastic deformations already observed by the evolution of $u_b - u_s$ depicted in Fig. 9. Based on this ideally-plastic material response no local failure mode over the anchor head developed. The remaining regions characterized by $\alpha_h = 1$ show low values for the hydrostatic pressure resulting in softening material behavior. Similar to the crack pattern obtained from the multi-surface model (Fig. 8), these regions refer to two circumferential cracks starting at the anchor head, and radial cracks propagating from the concrete surface into the interior of the concrete block.

4. Conclusions

In this paper, structural failure of anchor bolts placed in concrete was investigated. For this purpose, two material models for plain concrete were used.

One of them was a single-surface and the other one a multi-surface model. The latter model was originally proposed by MESCHKE [10] (it is referred to as *original* model). This model was reformulated in order to account for the influence of confinement. The reformulated model is referred to as *modified* multi-surface model. From the numerical simulations, the following conclusions concerning the structural response of the concrete specimen can be drawn:

- the concrete located between the anchor head and the support ring is subjected to strong non-uniform triaxal stress states, characterized by
  - hydrostatic pressure over the anchor head,
  - a compressive strut from the anchor head to the support ring, and
  - circumferential cracking caused by tensile loading perpendicular to this strut;
- the underlying material model has a crucial influence on the predicted failure mode characterized either
  - by local compressive failure over the anchor head, or
  - by a cone-shaped failure surface in consequence of the development of circumferential cracks.

The cone-shaped failure surface, which presumably represents the correct failure mode, was obtained by the *modified* multi-surface model and the single-surface model. The respective peak loads deviated by 8%. Disregard of the influence of confinement on the material strength and ductility in the context of the *original* multi-surface model resulted in local compressive failure of concrete over the anchor head. The peak load related to this presumably incorrect failure mode was found to be significantly lower than the peak loads obtained from the analyses characterized by cone-shaped failure.

References

1. L. ELFGREN, *Fracture mechanics of concrete structures,* Technical report, RILEM, Technical Committee 90, 1990.
2. G. ETSE, *Theoretische und numerische Untersuchung zum diffusen und lokalisierten Versagen in Beton,* [in German], PhD thesis, Universität Karlsruhe, Karlsruhe, 1992.
3. G. ETSE, *Finite element analysis of failure response behavior of anchor bolts in concrete,* Int. Journal of Nuclear Engineering and Design, 179, 245–252, 1998.
4. G. ETSE and K. WILLAM, *Fracture energy formulation for inelastic behavior of plain concrete,* Journal of Engineering Mechanics (ASCE), 120, 1983–2011, 1994.
5. CH. HELLMICH, F.-J. ULM, and H. A. MANG. *Consistent linearization in finite element analysis of coupled chemo-thermal problems with exo- or endothermal reactions,* Computational Mechanics, **24**, 4 238–244, 1999.
6. A. HILLERBORG, M. MODEER, and P.E. PETERSSON, *Analysis of crack formation and crack growth in concrete by means of fracture mechanics and finite elements,* Cement and Concrete Research, **6**, 773–782, 1976.

7. G. HOFSTETTER, J.C. SIMO, and R.L. TAYLOR, *A modified cap model: closest point solution algorithms,* Computers & Structures, **46**, 2, 203–214, 1993.

8. B. HURLBUT, *Experimental and computational investigation of strain-softening in concrete,* Master's thesis, University of Colorado, Boulder, USA, 1985.

9. H.A. MANG, R. LACKNER, P. PIVONKA, and CH. SCHRANZ, *Selected topics in computational structural mechanics,* In W.A. Wall, K.-U. Bletzinger, and K. Schweizerhof, editors, Trends in Computational Structural Mechanics, Lake Constance, Austria / Germany, pages 1–25, 2001.

10. G. MESCHKE, *Consideration of aging of shotcrete in the context of a 3D viscoplastic material model,* International Journal for Numerical Methods in Engineering, **39**, 3123–3143, 1996.

11. G. MESCHKE, R. LACKNER, and H.A. MANG, *An anisotropic elastoplastic-damage model for plain concrete,* International Journal for Numerical Methods in Engineering, **42**, (4):703–727, 1998.

12. M. ORTIZ, *A constitutive theory for the inelastic behavior of concrete,* Mech. of Materials, **4**; 67–93, 1985.

13. P. PIVONKA, R. LACKNER, and H. MANG, *Numerical analysis of concrete subjected to triaxial compressive loading,* [in:] CD-ROM Proceedings of the European Congress on Computational Methods in Applied Sciences and Engineering, Barcelona, Spain, 2000.

14. S. SMITH, *On fundamental aspects of concrete behavior,* Master's thesis, University of Colorado, Boulder, USA, 1987.

15. K. WILLAM and E. WARNKE, *Constitutive models for the triaxial behavior of concrete,* [in:] Int. Assoc. Bridge Struct. Eng. Sem. Concr. Struct. Subjected Triaxial Stresses, volume 19, pages 1–30, Bergamo, Italy, 1975. Int. Assoc. Bridge Struct. Eng. Proc.

Received May 20, 2001.